Published in final edited form as:
Biochemistry. 2013 March 5; 52(9): 1594–1602. doi:10.1021/bi3015482.

Inverse solvent isotope effects arising from substrate triggering in the factor inhibiting HIF (FIH-1)

John Hangasky[1], **Evren Saban**[1], and **Michael J. Knapp**[1]

Michael J. Knapp: mknapp@chem.umass.edu

[1]Department of Chemistry, University of Massachusetts, Amherst, MA, 01003 Voice 413-545-4001, FAX 413-545-4490

Abstract

Oxygen homeostasis plays a critical role in angiogenesis, erythropoiesis and cell metabolism. Oxygen homeostasis is set by the hypoxia inducible factor-1α (HIF-1α) pathway, which is controlled by Factor Inhibiting HIF-1α (FIH). FIH is a non-heme Fe(II), α-ketoglutarate dependent dioxygenase that inhibits HIF-1α by hydroxylating the C-terminal transactivation domain (CTAD) of HIF-1α at HIF-Asn^{803}. A tight coupling between CTAD binding and O_2-activation is essential for hypoxia sensing, making changes in the coordination geometry of Fe(II) upon CTAD encounter a crucial feature of this enzyme. Although the consensus chemical mechanism for FIH proposes that CTAD binding triggers O_2-activation by causing the Fe(II) cofactor to release an aquo ligand, experimental evidence of this point has been absent. More broadly, this proposed coordination change at Fe(II) has not been observed during steady-state turnover in any αKG oxygenase to date. In this manuscript, solvent isotope effects (SIEs) were used as a direct mechanistic probe of substrate triggered aquo release in FIH, as inverse SIEs (SIE < 1) are signatures for pre-equilibrium aquo release from metal ions. Our mechanistic studies of FIH have revealed inverse solvent isotope effects in the steady-state rate constants at limiting concentrations of CTAD or αKG: $^{D2O}k_{cat}/K_{M(CTAD)}$ = 0.40 ± 0.07, $^{D2O}k_{cat}/K_{M(\alpha KG)}$ = 0.32 ± 0.08, providing direct evidence for aquo release during steady-state turnover. Furthermore, the SIE at saturating concentrations of CTAD and αKG was inverse, $^{D2O}k_{cat}$ = 0.51 ± 0.07, indicating that aquo release occurs after CTAD binds. The inverse kinetic SIEs observed in the steady state for FIH can be explained by a strong Fe-OH_2 bond. The stable Fe-OH_2 bond plays an important part in FIH's regulatory role over O_2 homeostasis in humans, and points toward a strategy for tightly coupling O_2-activation with CTAD hydroxylation that relies on substrate triggering.

Introduction

Oxygen homeostasis is essential for proper cellular function in humans and is tightly controlled by a small group of non-heme Fe(II), alpha-ketoglutarate (αKG)-dependent dioxygenases. Oxygen-dependent regulation of the transcriptional coactivator hypoxia

Correspondence to: Michael J. Knapp, mknapp@chem.umass.edu.

Supporting Information

Supporting Information Available: Control experiments showing the effect of ionic strength and viscosity on the steady state kinetics of FIH. This material is available free of charge via the Internet at http://pubs.acs.org.

inducible factor-1α (HIF-1α) maintains O_2 homeostasis as HIF-1α controls more than 100 genes, directing processes such as angiogenesis, glycolysis and erythropoeisis.(1–3) The Fe(II)/αKG-dependent dioxygenase 'factor inhibiting HIF-1α' (FIH-1 or FIH) inhibits HIF-1α in the presence of sufficient [O_2] by hydroxylating the C-terminal activation domain (CTAD) of HIF-1α at HIF-Asn^{803}.(4–7) This hydroxylation prevents recruitment of the CREB binding protein, effectively down regulating HIF-1α dependent gene expression in response to normal or elevated [O_2].

The consensus mechanism for Fe(II)/αKG-dependent dioxygenases proposes that binding of primary substrate triggers the Fe(II) to bind O_2, due to aquo release opening a coordination site for O_2 (Scheme 1). Substrate triggering is a central tenet of the consensus mechanism, as it can explain the relative O_2-reactivity of αKG oxygenases. (11)(49) Subsequent O_2 activation allows for oxidative decarboxylation of αKG and the formation of a highly reactive ferryl intermediate. H-atom abstraction and ensuing •OH rebound effectively hydroxylates the primary substrate. As sensing [O_2] requires that O_2-activation only occur when HIF-1α is bound, substrate triggering is the key to O_2-sensing by FIH.

Various experimental techniques have been used to test the consensus mechanism of the Fe(II)/αKG-dependent dioxygenases. Extensive spectroscopic studies on the Fe(II)/αKG-dependent dioxygenase clavaminate synthase (CAS) have provided insight to the coordination change due to aquo release induced by primary substrate. MCD and CD studies of (Fe + αKG)CAS indicate the Fe(II) is predominantly 6 coordinate. Upon addition of primary substrate (*S*) the active site iron of (Fe + αKG + S)CAS adopts a 5 coordinate square-pyramidal geometry (8–10) due to release of the aquo ligand. Stopped-flow and freeze-quench techniques have been used to study the Fe(II)/αKG-dependent dioxygenase, taurine dioxygenase (TauD). Loss of the aquo ligand was observed under single-turnover conditions, and these studies identified a Fe(IV)=O intermediate as the active oxidant in TauD.(11–13) However these studies did not address aquo release under multiple turnover conditions leaving open the possibility that aquo release is not a recurring step in the steady-state.

To date, neither in depth spectroscopic studies of the coordination changes proposed upon substrate binding, nor mechanistic probes for substrate triggering have been reported for FIH, making substrate triggering in this enzyme largely speculative. The X-ray crystallographic data for FIH bound to various substrates is ambiguous with respect to the coordination geometry of Fe(II), making it difficult to draw conclusions about the link between substrate binding and aquo release. Structures of (Fe + αKG)FIH are reported as containing either 5-coordinate(15) or 6-coordinate(16) Fe(II), however the crystal structure of (Fe + αKG + CTAD)FIH shows a 5-coordinate Fe(II),(15) suggesting that aquo release may partially occur prior to CTAD binding. EPR spectroscopy of Co(II)-substituted (Co + αKG)FIH revealed a mixture of 5-coordinate and 6-coordinate Co(II), further suggesting that aquo release may occur prior to CTAD binding.(17, 18) Crystal structures of both (Fe + αKG + Notch)FIH and (Fe + αKG + TNKS2)FIH were refined with an axial aquo ligand present, suggesting that aquo release occurs *after* these substrates bind.(19, 20) Direct mechanistic probes of aquo release during turnover would provide a crucial view into the

mechanism of this enzyme, as well as providing insight into substrate triggering by this broad class of enzymes.

We propose that the extensive H-bonding network surrounding the active site of FIH constitutes a second coordination sphere, which transduces CTAD binding into aquo release. Steady-state kinetics of FIH point mutants indicate that removal of hydrogen-bonds from several residues surrounding the Fe(II) impairs catalytic efficiency(14), suggesting that substrate binding causes alterations to those hydrogen bonds. FIH has been shown to have a tightly coupled oxidative and reductive half reaction, avoiding the formation of reactive oxygen species during turnover.(21) Point mutations that perturb this H-bonding network significantly decrease FIH activity and lead to uncoupled αKG consumption.(14) Based on FIH crystal structures and mechanistic data for point mutants, we hypothesized that aquo release occurs on every turnover during the steady state.

To test this hypothesis, we applied mechanistic probes that are sensitive to those steps preceding O_2-activation. Specifically, we focused on the steps involving αKG and CTAD binding, as these steps lead to substrate triggering: the aquo release and priming of the Fe(II) for O_2 binding/activation. Steady-state kinetic assays were performed to identify the preferred binding order for CTAD and αKG. Solvent isotope effects (SIEs) on steady-state rate constants were measured to test for the release of aquo ligands from the Fe(II) cofactor. When the rate constants are larger in D_2O-containing buffers than for H_2O-containing buffer, the kinetics SIEs are ‘inverse’ and are diagnostic for pre-equilibrium release of aquo ligands from metal cofactors. We observed inverse SIEs on steady-state rate constants, providing direct evidence for the pre-equilibrium release of 1, 2 and 3 aquo ligands from the Fe(II) under different conditions. Our results establish two very important points. First, CTAD-binding to (Fe + αKG)FIH leads to release of 1 aquo ligand, suggesting that the overall strategy to control hydroxylation in FIH relies on substrate triggered changes in hydrogen-bonding to release the aquo ligand. Second, the rate-limiting step in the steady-state precedes or coincides with the first irreversible step – this is likely to be decarboxylation (Scheme 1), meaning that FIH does not accumulate oxidized intermediates. Both observations point to an overall strategy for O_2-activation that relies on careful control over substrate triggering in FIH.

Experimental Procedures

Materials

All buffers and reagents were purchased from commercial vendors and were not further purified, with the exception of the CTAD peptide. The CTAD peptide corresponding to the C-terminal activation domain of human HIF-1α, (HIF-1α$^{788–826}$) contained a Cys^{800} → Ala point mutation(21): DESGLPQLTSYDAEVN**A**APIQGSRNLLQGEELLRALDQVN. The CTAD peptide was purchased as a desalted peptide from EZBiolab (Carmel, IN, USA) with free N and C-termini. RP-HPLC utilizing a gradient from 30% acetonitrile/0.1% trifluoroacetic acid (TFA) to 95% acetonitrile/0.1% TFA was used to obtain CTAD of >95% purity.

Protein Expression and Purification

FIH was overexpressed in *E. coli* with an N-terminal His_6 tag and purified as previously described.(18) Briefly, His_6-FIH was separated from cell lysate via Ni-NTA column chromatography and the affinity tag was then cleaved with thrombin. Three additional residues, from the fusion protein (NH_2-GlySerHis-) remained on the N-terminus following thrombin cleavage. Cleaved FIH was collected as flow through from a Ni-NTA column and then incubated with EDTA to removed metal. Dimeric FIH was obtained with size-exclusion chromatography using Sephadex G-75 resin and 50 mM NaCl 50 mM Tris pH 8.00 as the running buffer. Purified FIH was buffer exchanged into 50 mM HEPES pH 7.00. The molecular weight was confirmed by QSTAR TOF-MS (expected, 40.566 kDa; observed, 40.574 kDa), while the purity (>95%) was assessed by SDS-PAGE.

Steady-state kinetics assays

All assays were performed at 37.0°C with saturating concentrations of $FeSO_4$ (50 μM) and ascorbate (2 mM), and ambient O_2 concentration. Assays in which CTAD was the varied substrate (15 μM – 250 μM) utilized saturating αKG (500 μM) unless specified otherwise. Assays with αKG as the varied substrate (5 μM – 200 μM) utilized a fixed CTAD concentration of either 39 μM (~1/2$K_{M(CTAD)}$) or 306 μM (~4x$K_{M(CTAD)}$). Assay reagents were mixed and incubated for two minutes at 37.0°C in microcentrigue tubes. Then the reaction was initiated with the addition of enzyme ($[E]_T$ = 0.5 μM). Reaction aliquots (5 μL) were quenched with 75% acetonitrile/0.2% TFA (20 μL) saturated with 3,5-dimethoxy-4-hydroxycinnamic acid and analyzed for peptide hydroxylation using a Bruker Daltonics Omniflex MALDI-TOF-MS. The mole fraction of product, $\chi_{CTAD\text{-}OH}$, was determined by the relative intensities of hydroxylated CTAD ($CTAD^{OH}$, 4271 m/z) and unhydroxylated CTAD (4255 m/z). Initial rates were determined from 5–7 quenched timepoints. The steady-state rate constants, k_{cat} and k_{cat}/K_M, were obtained by nonlinear least-squares fitting of initial rate data (0 to ~15% fractional conversion) to the Michaelis-Menten equation.

Viscosity Assays

Steady-state assays were performed in 50 mM HEPES pH 7.00, using sucrose as the viscosogen to test for the rate limitation of diffusional steps. Initial rates were measured as described above, using buffers containing 10% (η_{rel}=1.3), 18% (η_{rel}=1.8) and 25% (η_{rel}=2.8) sucrose solutions (w/w).(22)

Solvent Isotope Assays

Deuterium oxide (D, 99.9%) was purchased from Cambridge Isotope Laboratories (Andover, MA, USA) and used as received. The pD was determined by pre-soaking the pH meter in D_2O for ten minutes and then adding 0.4 to the meter reading of the D_2O solution of interest (pD = pH_{read} + 0.4).(23) Steady-state assays were performed as described above. All reagent stocks used in the steady-state assays in D_2O, were prepared using D_2O. Working FIH stock solutions were made by diluting high concentration stocks from H_2O into D_2O containing 50mM HEPES pD 7.00. Assays were performed in 50 mM HEPES, pD 7.00, with a final D_2O percentage of 97%. SIEs were calculated from the ratio of rate constants observed in buffers containing H_2O or D_2O; e.g. $^{D2O}k_{cat} = k_{cat(H2O)}/k_{cat(D2O)}$.

Coupling Ratio

The extent of coupling between FIH's two half reactions in D_2O was determined from monitoring the succinate and $CTAD^{OH}$ concentrations throughout a reaction. Reactions containing αKG (500 μM), $FeSO_4$ (50 μM), CTAD (200 μM) and FIH (5 μM) were performed in 50 mM Tris pD 7.00, and analyzed similarly to previously reported procedures.(14, 24) A Hamilton PRP-X300 anion exclusion column was used to separate the succinate produced from the quenched reactions. UV detection at 210 nm was used to determine the succinate concentration. Using aliquots from the same quenched assay, a Bruker Daltonics Omniflex MALDI-TOF-MS was used to determine the $CTAD^{OH}$ concentration. The coupling ratio (*C*) was determined by fitting [succinate] as a linear function of [$CTAD^{OH}$] for multiple quench points, where *C* = [succinate]/[$CTAD^{OH}$].

Results

Solvent isotope effects

Solvent isotope effects (SIEs) were measured to test for aquo release from the Fe(II) as part of substrate triggering during turnover in FIH. By varying the degree of saturation with respect to αKG and CTAD, the SIE on kinetic constants reporting on different microscopic steps were accessed. SIEs arising from the pre-equilibirum release of 1, 2, and 3 aquo ligands were predicted from the consensus mechanism, depending on the assay conditions (Scheme 1). As the limiting SIEs are multiples of the proton fractionation factor (Φ) for the O-L bond (L = H or D)(25), they are quite distinct for the number of aquo ligands released.

The fractionation factor for L_2O (where L = H or D) is inverse when water is bonded to another Lewis acid, leading to a tendency for D_2O to accumulate in bulk solvent. For example, $\Phi_{O\text{-}L} = 0.69$ for L_3O^+ (26–28) due to zero-point energy differences. The fractionation factor, $\Phi_{O\text{-}L}$, for aquo release from Co(II) in two carbonic anhydrase isozymes has been found to be between 0.72 and 0.90,(25, 29) agreeing closely with the fractionation factor for $Co(H_2O)_6^{2+}$ in solution, ($\Phi_{O\text{-}L} = 0.73$).(30) As the fractionation factor for the Fe^{2+}-OH_2 in FIH is unknown, we estimate $\Phi = 0.70$ as is commonly done for fractionation of water from other M-OH_2 $\rightleftharpoons$ M + OH_2 equilibria.(30) As Φ is reported on a per-bond basis, and are multiplicative, $^{D2O}K_{eq}$ for the release of aquo ligands are diagnostic for the numbers of H_2O released from Fe: one ($^{D2O}K_{eq} = \Phi^2 = 0.49$), two ($^{D2O}K_{eq} = \Phi^4 = 0.24$) and three ($^{D2O}K_{eq} = \Phi^6 = 0.12$).

The *equilibrium* fractionation factors will lead to inverse *kinetic* SIEs on different kinetic constants provided that the aquo release is in a pre-equilibrium prior to a subsequent rate-limiting step. As shown in the Appendix, k_{cat} and $k_{cat}/K_{M(CTAD)}$ can report on one aquo release – leading to the prediction that the limiting values for $^{D2O}k_{cat} \sim {}^{D2O}(k_{cat}/K_{M(CTAD)}) = 0.49$. In contrast, the limiting values for $^{D2O}(k_{cat}/KM_{(\alpha KG)})$ will report on the release of 2 or 3 aquo ligands depending on the degree to which FIH is saturated with CTAD. It is important to note that our assays used ambient [O_2] (220μM), which is approximately $2xK_{M(O2)}$,(31) making our kinetic constants apparent.

The rate constants obtained under conditions of saturating αKG, ambient [O_2] and varied [CTAD] are k_{cat} and $k_{cat}/K_{M(CTAD)}$. Under these conditions, k_{cat} reports on all steps after CTAD binding up through product release, and is predicted to involve the release of one aquo ligand.(Scheme 1) The initial rate assays in D_2O exhibited increased rates when compared to similar assays in H_2O, indicating an inverse SIE on both k_{cat} and $k_{cat}/K_{M(CTAD)}$. We observed $^{D2O}k_{cat} = 0.51 \pm 0.07$, in good agreement with the limiting SIE (0.49) for the pre-equilibrium release of one aquo ligand (Figure 1). Similarly, we observed $^{D2O}(k_{cat}/K_{M(CTAD)}) = 0.40 \pm 0.07$, which is also in good agreement with one aquo release prior to a rate-limiting step.

Due to the sequential ordered mechanism (see below), the apparent $k_{cat}/K_{M(\alpha KG)}$ encompasses distinct steps depending on the fixed concentration of CTAD. Since $k_{cat}/K_{M(\alpha KG)}$ reports on steps from the encounter with αKG up through the first irreversible step, high or low fixed concentrations of CTAD were used to isolate different microscopic steps. CTAD binding is kinetically irreversible at high CTAD concentrations, meaning that $k_{cat}/K_{M(\alpha KG)High[CTAD]}$ reports on only those steps between αKG encounter and CTAD binding, encompassing the release of two aquo ligands. The observed SIE of 0.32 ± 0.08 on $k_{cat}/K_{M(\alpha KG)High[CTAD]}$ was in reasonable agreement with the limiting value (0.24) expected for the release of two aquo ligands. In contrast, CTAD binding is kinetically reversible at sub-saturating CTAD concentrations, making a subsequent step (thought to be O_2 activation) the first irreversible step. Thus, $k_{cat}/K_{M(\alpha KG)Low[CTAD]}$ reports on all steps between αKG binding and O_2 activation, which encompasses the release of three aquo ligands in the consensus mechanism. The observed SIE of 0.11 ± 0.03 for $k_{cat}/K_{M(\alpha KG)Low[CTAD]}$ agreed closely with the limiting value (0.12) expected for the release of three aquo ligands prior to a rate-limiting step (Figure 2).

Validation of Observed SIEs

A series of control experiments were completed to ensure that the SIEs arose from aquo release. Control assays showed the steady-state rate constants, k_{cat} and $k_{cat}/K_{M(CTAD)}$, were pH independent between pH 6.50 and pH 8.00 at fixed ionic strength (I = 120 mM). Furthermore, steady-state assays at pH 7.00 showed that k_{cat} and $k_{cat}/K_{M(CTAD)}$ were independent of ionic strength (Figure S1). Viscosity experiments were completed as a control for the increased relative viscosity of D_2O, as solvent viscosity can affect the rate of diffusional steps, or of conformational changes. The binding order of αKG and CTAD was also investigated to define the chemical steps reported on by $k_{cat}/K_{M(CTAD)}$ and $k_{cat}/K_{M(\alpha KG)}$, as these rate constants proved different microscopic steps within the chemical mechanism reporting the release of up to three aquo ligands.

FIH's activity increased approximately two fold in D_2O, prompting us to check the coupling between the oxidative and reductive half-reactions in D_2O. As the oxidative half reaction produces succinate, and the reductive half-reaction produces $CTAD^{OH}$, the [succinate]/[$CTAD^{OH}$] ratio is equal to the coupling between these half reactions (C=[succinate]/[$CTAD^{OH}$]). Previously we showed tight coupling between succinate production and CTAD hydroxylation in H_2O.(14) Here we observed that FIH's two half reactions remained tightly

coupled in D_2O, with *C* equal to unity within experimental uncertainty($C = 1.1 \pm 0.1$) (Table 2).

Diffusional steps are not rate-limiting

Steady-state rate constants were measured as a function of relative viscosity to test for diffusional steps that might contribute to the observed rate constants and SIEs, as the viscosity of D_2O is greater than that of H_2O. Initial rate data were collected in 50 mM HEPES, pH 7.00, with sucrose as the viscosogen, and fitted to the Michaelis-Menten equation. Analysis of k_{cat}, $k_{cat}/K_{M(CTAD)}$ and $k_{cat}/K_{M(\alpha KG)}$ as a function of relative viscosity indicated that each of the steady-state rate constants were independent of solvent viscosity (Figure S2).

The normalized regression plot showed that relative viscosity had no effect on any rate constant. Thus, neither diffusional encounter, relevant for k_{cat}/K_M, nor product release, relevant for k_{cat}, are rate-limiting. If diffusional encounter were rate limiting, k_{cat}/K_M would decrease as the relative solvent viscosity increased.(32, 33) Furthermore, the lack of a viscosity effect indicates FIH does not undergo a viscosity-sensitive conformational change, which has been shown to obscure SIEs for some enzymes.(34, 35)

Sequential Order: αKG binds before CTAD

The consensus mechanism for αKG oxygenases is a sequential ordered model that, when applied to FIH, predicts αKG binds prior to CTAD. Although steady-state analyses of several other αKG-dependent oxygenases have been shown to follow this binding order, (36–38) we tested this sequential binding model for FIH due to the interesting SIEs that we observed under varied [CTAD]. As the binding order of αKG and CTAD affects the microscopic steps defined by the steady-state kinetic parameters, this is critical to our interpretations of the SIEs.

Four different fixed CTAD concentrations, ranging from $½K_{M(CTAD)}$ to $4xK_{M(CTAD)}$ were chosen for steady state kinetic assays where the αKG concentration was the varied substrate. In close agreement with previously reported values,(14, 31) the $K_{M(\alpha KG)}$ remained constant at 20 ± 2μM for all CTAD concentrations. The regression plot of $k_{cat}/K_{M(\alpha KG)}$ as a function of [CTAD] passed through the origin, as expected for ordered sequential binding of αKG prior to CTAD (Figure 3).(39)

Discussion

O_2 sensing by FIH is critical to cellular growth and development making close consonance between [O_2] and the FIH-catalyzed hydroxylation of CTAD central to O_2-homeostasis. An additional benefit is that controlled O_2 activation by FIH would avoid ROS production (21), preventing anomalous oxidations. Although it has been shown that decarboxylation of αKG and hydroxylation of CTAD by FIH is tightly coupled,(14) the mechanistic strategy used by FIH to ensure that O_2 activation leads to CTAD hydroxylation with high fidelity remains unclear. Our overall hypothesis is the hydrogen bonding from the second coordination sphere ensures that the Fe(II) in (Fe + αKG)FIH remains 6-coordinate, and that CTAD binding alters these hydrogen bonds leading to O_2 activation – the substrate triggering

model. CTAD binding could trigger FIH by affecting any one of the microscopic steps in the overall chemical mechanism, so long as the rate of O_2-activation were increased upon CTAD binding. Our observation of inverse SIEs on $k_{cat}/K_{M(CTAD)}$ and $k_{cat}/KM_{(\alpha KG)}$ indicate that the rate-limiting step in the steady state follows aquo release, and is either coincident with or precedes decarboxylation (Scheme 1). This points towards a strategy for tightly coupling O_2-activation with CTAD hydroxylation that relies on substrate triggering.

O_2-activation is rate-limiting in FIH

Inverse kinetic SIEs (SIE < 1) are diagnostic for aquo release from metal ions, as the vast majority of SIEs are normal (SIE > 1).(29) Two other causes of inverse kinetic SIEs, the involvement of a CysS- nucleophile in catalysis, and a conformational change, were ruled out for FIH. In the former case, there are no active site CysSH residues; in the latter case, we verified that viscosity did not affect the rate of turnover.

Inverse kinetic SIEs have been reported for several metalloenzymes, including a number of hydrolases, carbonic anhydrase, and a point mutant of SLO.(29, 40–43) In each case, the inverse kinetic SIEs indicated that aquo release was a pre-equilibrium step prior to a subsequent rate limiting step. Our observation of inverse kinetic SIEs corresponding to multiple aquo release steps is the first such report, to the best of our knowledge. The inverse SIEs arise from an unfavorable equilibrium for aquo release, combined with a slow O_2 activation step.

The consensus mechanism predicts that both k_{cat} and $k_{cat}/K_{M(CTAD)}$ encompass one aquo release for a limiting predicted SIE = 0.49. The experimentally observed kinetic SIEs correlate nicely with the theoretical value expected for the equilibrium release of one aquo ligand, as $^{D2O}k_{cat} = 0.51 \pm 0.07$ and $^{D2O}k_{cat}/K_{M(CTAD)} = 0.40 \pm 0.07$.(Table 1) A kinetic model with separate microscopic steps for αKG, CTAD and O_2 binding, as well as the final aquo release, was constructed from the consensus chemical mechanism and used to analyze the observed SIEs (Scheme 2). As k_{cat} encompasses all steps with the exception of diffusional encounter with substrates, a separate, reversible microscopic step for aquo release was needed, as the $^{D2O}k_{cat} < 1$ indicated that aquo release must be separate from CTAD encounter.

The similarity in the SIEs for k_{cat} and $k_{cat}/K_{M(CTAD)}$ strongly suggests that the overall rate-limiting step in FIH turnover is common to both rate constants. As $k_{cat}/K_{M(CTAD)}$ encompasses steps between CTAD encounter and the first irreversible step, the common step has to be the O_2-activation step (Scheme1). This step is typically viewed as the initial attack on the 2-oxo group of αKG which leads to oxidative decarboxylation. This is noteworthy as that this predicts that FIH will not accumulate the ferryl intermediate during turnover, in contrast to TauD.(12) Slow O_2-activation can account for the tight coupling between decarboxylation and hydroxylation seen for FIH(14) as hydroxylation must be very fast relative to the decarboxylation step. Thus, we conclude that FIH likely adopts a strategy to ensure tight coupling between O_2-binding and -activation in which O_2-activation is rate-limiting.

We analyzed the observed kinetic SIEs using language predominately developed by Northrop and Cleland (44, 45), in which observed kinetic SIEs are a function of "commitments to catalysis" and the equilibrium and kinetic isotope effects ($^{D2O}K_{qq}$ and $^{D2O}k_5$) on the aquo release step (k_5). The commitments to catalysis, C_f and C_r, are ratios of microscopic rate constants that describe the tendency of an enzyme to go forward or backward through the isotopically sensitive step. Full expressions are provided in the Appendix. In the case of $^{D2O}k_{cat}/K_{M(CTAD)}$, this expression takes the form below. The primary virtue of such a presentation is that it permits us to focus on specific segments of the kinetic mechanism. As equilibrium isotope effects reflect fractionation factors, the equilibrium SIE on aquo release is predicted to be ~ 0.5 ($^{D2O}K_5 = 0.49$).

$$^{D2O}\left(\frac{k_{cat}}{K_{M(CTAD)}}\right)=\frac{^{D2O}k_5+C_f+C_r\,^{D2O}K_5}{1+C_f+C_r} \quad (1)$$

It is clear that the only way for $^{D2O}k_{cat}/K_{M(CTAD)} = {}^{D2O}K_{eq}$ is for the reverse commitment to be very large ($C_r \gg C_f$). Reverse commitment (C_r) is the kinetic competition between H_2O and O_2 for the triggered form of enzyme – when C_r is large, it means that H_2O is the preferred ligand (Appendix – Eqn. A10). Furthermore, the C_f/C_r ratio is, to a first approximation, the equilibrium for aquo release – when $C_f/C_r \ll 1$, it means that K_5 is much less than one and that the position of this equilibrium favors the aquo-on state. Similar analysis of the commitment factors for $^{D2O}k_{cat}$ further supports the conclusion that aquo release is disfavored thermodynamically, despite a slightly different SIE expression and forward commitment on k_{cat} (C_{vf}) (Appendix).

Substrate triggering is faster than O_2-activation

Steps involved in substrate triggering were accessed by measuring the kinetic SIE with sub-saturating [αKG]. As $k_{cat}/K_{M(\alpha KG)}$ includes steps between diffusional encounter of αKG with FIH, up through and including the subsequent irreversible step, CTAD binding and substrate triggering may be observable on this kinetic constant. Under conditions of high [CTAD], only the two aquo ligands released upon αKG binding may be observed, as saturating FIH with CTAD makes CTAD binding kinetically irreversible for $k_{cat}/K_{M(\alpha KG)High[CTAD]}$. In contrast, subsaturating [CTAD] makes it possible to access release of all three aquo ligands on $k_{cat}/K_{M(\alpha KG)Low[CTAD]}$, provided that a later step be rate-limiting.

The observed SIE for $k_{cat}/K_{M(\alpha KG)High[CTAD]}$ (SIE = 0.32 ± 0.08) correlates well with the pre-equilibrium release of two aquo ligands (Table 1), as expected for kinetically irreversible CTAD binding. The key observation supporting rapid substrate triggering was the SIE on $k_{cat}/K_{M(\alpha KG)Low[CTAD]}$ (SIE = 0.11 ± 0.03), as this indicated the pre-equilibrium release of all three aquo ligands prior to a subsequent rate-limiting step. This establishes that steps associated with CTAD binding and substrate triggering are not slow under these conditions, and further points to O_2-activation as the rate-limiting step.

Hydrogen bonding from the second coordination sphere

Turnover in FIH and other αKG oxygenases depends on substrate triggering – minimally the release of the aquo ligand from the (Fe + αKG + Substr) enzyme form – prior to O_2 binding. What is striking about the kinetics of FIH are the inverse kinetic SIEs, implicating slow O_2-activation in this enzyme. In the case of FIH, substrate triggering leads to *rate-limiting* O_2-activation, meaning that the intermediate which is expected to accumulate in the steady-state is a relatively innocuous Fe^{2+} center. In contrast, TauD exhibits SIEs of unity(46), and the partially rate-limiting steps include product release and H-atom transfer by the $[Fe^{IV}O]^{2+}$ intermediate.(11) For TauD, substrate triggering leads to *rapid* O_2-activation, and the partial accumulation of a powerful oxidant, $[Fe^{IV}O]^{2+}$.(12) It is as if TauD were built for speed, but FIH built for fidelity. As the ligands to the Fe(II) are identical in these two enzymes, the reasons for such disparate strategies for the oxidation reaction must lie beyond the primary coordination sphere.

We attribute the difference in oxidation strategies between these enzymes to their second coordination spheres. The most striking difference between their second coordination spheres is in the hydrogen bonding between the facial triad Asp^{201} ligand and the axial aquo ligand. In FIH, the remote O-atom of Asp^{201} forms a 2.8 Å hydrogen bond to the bound aquo ligand in (Fe + αKG)FIH (Figure 4) – once CTAD binds, two new hydrogen bonds form to the Asp^{201} which appear to serve to partially stimulate aquo release.(16, 17) The extensive hydrogen bonding to this aquo ligand likely serves to stabilize the Fe-OH_2 bond, which would explain the large reverse commitments to catalysis (C_r) and the inverse SIEs. Such high affinity for the aquo ligand could serve to throttle back the oxidation reaction such that O_2-activation only occurs when CTAD is present. We note a certain similarity to the hydrogen bonding network found in PHD2, which leads to an inverse $^{D2O}k_{cat}$ (47) and the absence of any accumulating intermediates in pre-steady state experiments.(24)

TauD is a significant contrast to FIH, structurally and kinetically. The facial triad Asp of TauD is rotated away from the aquo ligand, and cannot form a hydrogen bond to the bound aquo ligand. This leads to a weak Fe^{2+}-OH_2 bond strength(48), and TauD readily activates O_2 in the absence of the substrate taurine.(49, 50) The second coordination sphere of TauD favors aquo-release, which can lead to rapid O_2-activation – unfortunately, this leads to a reduction in fidelity.

Conclusion

Inverse kinetic SIEs on k_{cat}/K_M and k_{cat} limit the possible rate-limiting step for FIH to a step between aquo release and decarboxylation (Scheme 1). This points to a step very early in the catalytic cycle, such as O_2 activation, as the likely rate-limiting step. Such a strategy would aid in FIH's regulatory role over O_2 homeostasis in humans, as it would lead to direct transduction of intracellular O_2 levels into a readable signal, hydroxylated HIF-Asn^{803}. This tight control over O_2-activation strongly suggests that oxidized intermediates will not accumulate in FIH under normal turnover conditions, and may reflect the demands of a regulatory function in O_2-sensing by tightly correlating O_2-activation with substrate hydroxylation.

Supplementary Material

Refer to Web version on PubMed Central for supplementary material.

Acknowledgments

We thank the NIH for funding (R01-GM077413).

Abbreviations

HIF	hypoxia inducible factor-1α
FIH	factor-inhibiting HIF
αKG	α-ketoglutarate
CTAD	C-terminal transactivation domain
CREB	cAMP response element-binding protein
CAS	clavaminate synthase
MCD	magnetic circular dichroism
CD	circular dichroism
HEPES	4-(2-hydroxyethyl)-1-piperazineethanesulfonic acid
SIE	solvent isotope effect
ROS	reactive oxygen species
PHD2	prolyl hydroxylase dioxygenase 2
TauD	taurine dioxygenase
SLO	soybean lipoxygenase

References

1. Hausinger RP. FeII/alpha-ketoglutarate-dependent hydroxylases and related enzymes. Crit Rev Biochem Mol Biol. 2004; 39:21–68. [PubMed: 15121720]
2. Solomon EI, Brunold TC, Davis MI, Kemsley JN, Lee SK, Lehnert N, Neese F, Skulan AJ, Yang YS, Zhou J. Geometric and electronic structure/function correlations in non-heme iron enzymes. Chem Rev. 2000; 100:235–350. [PubMed: 11749238]
3. Costas M, Mehn MP, Jensen MP, Que L Jr. Dioxygen activation at mononuclear nonheme iron active sites: enzymes, models, and intermediates. Chem Rev. 2004; 104:939–986. [PubMed: 14871146]
4. Hewitson KS, McNeill LA, Riordan MV, Tian YM, Bullock AN, Welford RW, Elkins JM, Oldham NJ, Bhattacharya S, Gleadle JM, Ratcliffe PJ, Pugh CW, Schofield CJ. Hypoxia-inducible factor (HIF) asparagine hydroxylase is identical to factor inhibiting HIF (FIH) and is related to the cupin structural family. J Biol Chem. 2002; 277:26351–26355. [PubMed: 12042299]
5. Ivan M, Kondo K, Yang H, Kim W, Valiando J, Ohh M, Salic A, Asara JM, Lane WS, Kaelin WG Jr. HIFalpha targeted for VHL-mediated destruction by proline hydroxylation: implications for O2 sensing. Science. 2001; 292:464–468. [PubMed: 11292862]
6. Lando D, Peet DJ, Gorman JJ, Whelan Da, Whitelaw ML, Bruick RK. FIH-1 is an asparaginyl hydroxylase enzyme that regulates the transcriptional activity of hypoxia-inducible factor. Genes Devel. 2002; 16:1466–1471.1. [PubMed: 12080085]

7. McNeill LA, Hewitson KS, Claridge TD, Seibel JF, Horsfall LE, Schofield CJ. Hypoxia-inducible factor asparaginyl hydroxylase (FIH-1) catalyses hydroxylation at the beta-carbon of asparagine-803. Biochem J. 2002; 367:571–575. [PubMed: 12215170]
8. Zhou J, Gunsior M, Bachmann BO, Townsend CA, Solomon EI. Substrate Binding to the α-Ketoglutarate-Dependent Non-Heme Iron Enzyme Clavaminate Synthase 2: Coupling Mechanism of Oxidative Decarboxylation and Hydroxylation. J Am Chem Soc. 1998; 120:13539–13540.
9. Zhou J, Kelly WL, Bachmann BO, Gunsior M, Townsend CA, Solomon EI. Spectroscopic studies of substrate interactions with clavaminate synthase 2, a multifunctional alpha-KG-dependent non-heme iron enzyme: Correlation with mechanisms and reactivities. J Am Chem Soc. 2001; 123:7388–7398. [PubMed: 11472170]
10. Pavel EG, Zhou J, Busby RW, Gunsior M, Townsend CA, Solomon EI. Circular dichroism and magnetic circular dichroism spectroscopic studies of the non-heme ferrous active site in clavaminate synthase and its interaction with alpha-ketoglutarate cosubstrate. J Am Chem Soc. 1998; 120:743–753.
11. Price JC, Barr EW, Hoffart LM, Krebs C, Bollinger JM. Kinetic dissection of the catalytic mechanism of taurine: alpha-ketoglutarate dioxygenase (TauD) from Escherichia coli. Biochemistry. 2005; 44:8138–8147. [PubMed: 15924433]
12. Price JC, Barr EW, Tirupati B, Bollinger JM Jr, Krebs C. The first direct characterization of a high-valent iron intermediate in the reaction of an alpha-ketoglutarate-dependent dioxygenase: a high-spin FeIV complex in taurine/alpha-ketoglutarate dioxygenase (TauD) from Escherichia coli. Biochemistry. 2003; 42:7497–7508. [PubMed: 12809506]
13. Price JC, Barr EW, Glass TE, Krebs C, Bollinger JM Jr. Evidence for hydrogen abstraction from C1 of taurine by the high-spin Fe(IV) intermediate detected during oxygen activation by taurine:alpha-ketoglutarate dioxygenase (TauD). J Am Chem Soc. 2003; 125:13008–13009. [PubMed: 14570457]
14. Saban E, Chen YH, Hangasky JA, Taabazuing CY, Holmes BE, Knapp MJ. The Second Coordination Sphere of FIH Controls Hydroxylation. Biochemistry. 2011; 50:4733–4740. [PubMed: 21456582]
15. Elkins JM, Hewitson KS, McNeill LA, Seibel JF, Schlemminger I, Pugh CW, Ratcliffe PJ, Schofield CJ. Structure of factor-inhibiting hypoxia-inducible factor (HIF) reveals mechanism of oxidative modification of HIF-1 alpha. J Biol Chem. 2003; 278:1802–1806. [PubMed: 12446723]
16. Dann CE, Bruick RK, Deisenhofer J. Structure of factor-inhibiting hypoxia-inducible factor 1: An asparaginyl hydroxylase involved in the hypoxic response pathway. Proc Natl Acad Sci USA. 2002; 99:15351–15356. [PubMed: 12432100]
17. Chen Y-H, Comeaux LM, Eyles SJ, Knapp MJ. Auto-hydroxylation of FIH-1, an Fe(II), α-ketoglutarate dependent human hypoxia sensor. Chem Commun. 2008:4768–4770.
18. Chen YH, Comeaux LM, Herbst RW, Saban E, Kennedy DC, Maroney MJ, Knapp MJ. Coordination changes and auto-hydroxylation of FIH-1: Uncoupled O-2-activation in a human hypoxia sensor. J Inorg Biochem. 2008; 102:2120–2129. [PubMed: 18805587]
19. Yang M, Chowdhury R, Ge W, Hamed RB, McDonough MA, Claridge TDW, Kessler BM, Cockman ME, Ratcliffe PJ, Schofield CJ. Factor-inhibiting hypoxia-inducible factor (FIH) catalyses the post-translational hydroxylation of histidinyl residues within ankyrin repeat domains. FEBS J. 2011; 278:1086–1097. [PubMed: 21251231]
20. Coleman ML, McDonough MA, Hewitson KS, Coles C, Mecinovic J, Edelmann M, Cook KM, Cockman ME, Lancaster DE, Kessler BM, Oldham NJ, Ratcliffe PJ, Schofield CJ. Asparaginyl hydroxylation of the notch ankyrin repeat domain by factor inhibiting hypoxia-inducible factor. J Biol Chem. 2007; 282:24027–24038. [PubMed: 17573339]
21. Saban E, Flagg SC, Knapp MJ. Uncoupled O_2-activation in the human HIF-asparaginyl hydroxylase, FIH, does not produce reactive oxygen species. J Inorg Biochem. 2011; 105:630–636. [PubMed: 21443853]
22. CRC Handbook of Chemistry and Physics. 61. CRC Press; Boca Raton: 1981.
23. Quinn, DM.; Sutton, LD. Theoretical Basis and Mechanistic Utility of Solvent Isotope Effects. In: Cook, PF., editor. Enzyme Mechanism from Isotope Effects. CRC Press; Boca Raton: 1991. p. 73-126.

24. Flashman E, Hoffart LM, Hamed RB, Bollinger JM, Krebs C, Schofield CJ. Evidence for the slow reaction of hypoxia-inducible factor prolyl hydroxylase 2 with oxygen. FEBS J. 2010; 277:4089–4099. [PubMed: 20840591]
25. Enzyme Mechanism from Isotope Effects. CRC Press; 1991.
26. McFarland J, Bernhard SA. Catalytic Steps During Single-Turnover Reduction of Aldehydes by Alcohol-Dehydrogenase. Biochemistry. 1972; 11:1486. [PubMed: 4336620]
27. Lee KM, Dahlhauser KF, Plapp BV. Reactivity of Horse Liver Alcohol-Dehydrogenase with 3-Methylcyclohexanols. Biochemistry. 1988; 27:3528–3532. [PubMed: 3390450]
28. Dunn MF, Hutchison JS. Roles of zinc ion and reduced coenzyme in the formation of a transient chemical intermediate during the equine liver alcohol dehydrogenase catalyzed reduction of an aromatic aldehyde. Biochemistry. 1973; 12:4882–4892. [PubMed: 4357551]
29. Kassebaum JW, Silverman DN. Hydrogen/deuterium fractionation factors of the aqueous ligand of cobalt in Co(H2O)62+ and Co(II)-substituted carbonic anhydrase. J Amer Chem Soc. 1989; 111:2691–2696.
30. Cook, PF. Enzyme Mechanism from Isotope Effects. CRC Press; Boca Raton: 1991. Kinetic and regulatory mechanisms of enzymes from isotope effects; p. 203-230.
31. Koivunen P, Hirsilä M, Günzler V, Kivirikko KI, Myllyharju J. Catalytic properties of the asparaginyl hydroxylase (FIH) in the oxygen sensing pathway are distinct from those of its prolyl 4-hydroxylases. J Biol Chem. 2004; 279:9899–9904. [PubMed: 14701857]
32. Blacklow SC, Raines RT, Lim Wa, Zamore PD, Knowles JR. Triosephosphate isomerase catalysis is diffusion controlled. Biochemistry. 1988; 27:1158–1167. [PubMed: 3365378]
33. Brouwer AC, Kirsch JF. Investigation of diffusion-limited rates of chymotrypsin reactions by viscosity variation. Biochemistry. 1982; 21:1302–1307. [PubMed: 7074086]
34. Raber ML, Freeman MF, Townsend CA. Dissection of the Stepwise Mechanism to β-Lactam Formation and Elucidation of a Rate-determining Conformational Change in β-Lactam Synthetase. J Biol Chem. 2009; 284:207–217. [PubMed: 18955494]
35. Karsten WE, Lai CJ, Cook PF. Inverse Solvent Isotope Effects in the NAD-Malic Enzyme Reaction Are the Result of the Viscosity Difference between D2O and H2O: Implications for Solvent Isotope Effect Studies. J Amer Chem Soc. 1995; 117:5914–5918.
36. Holme E. Kinetic study of thymine 7-hydroxylase from Neurospora crassa. Biochemistry. 1975; 14:4999–5003. [PubMed: 126696]
37. Rundgren M. Steady state kinetics of 4-hydroxyphenylpyruvate dioxygenase from human liver (III). J Biol Chem. 1977; 252:5094–5099. [PubMed: 873933]
38. De Carolis E, De Luca V. Purification, characterization, and kinetic analysis of a 2-oxoglutarate-dependent dioxygenase involved in vindoline biosynthesis from Catharanthus roseus. J Biol Chem. 1993; 268:5504–5511. [PubMed: 8449913]
39. Cook, PF.; Cleland, WW. Enzyme Kinetics and Mechanism. Garland Science; New York: 2007.
40. Izquierdo MC, Stein RL. Mechanistic studies of thermolysin. J Amer Chem Soc. 1990; 112:6054–6062.
41. Born TL, Zheng R, Blanchard JS. Hydrolysis of N-succinyl-L,L-diaminopimelic acid by the Haemophilus influenzae dapE-encoded desuccinylase: metal activation, solvent isotope effects, and kinetic mechanism. Biochemistry. 1998; 37:10478–10487. [PubMed: 9671518]
42. Harrison RK, Chang B, Niedzwiecki L, Stein RL. Mechanistic studies on the human matrix metalloproteinase stromelysin. Biochemistry. 1992; 31:10757–10762. [PubMed: 1420192]
43. Tomchick DR, Phan P, Cymborowski M, Minor W, Holman TR. Structural and Functional Characterization of Second-Coordination Sphere Mutants of Soybean Lipoxygenase-1. Biochemistry. 2001; 40:7509–7517. [PubMed: 11412104]
44. Cook PF, Cleland WW. Mechanistic deductions from isotope effects in multireactant enzyme mechanisms. Biochemistry. 1981; 20:1790–1796. [PubMed: 7013799]
45. Northrop, DB. Isotope Effects on Enzyme-Catalyzed Reactions. University Park Press; Baltimore, MD: 1977.
46. Grzyska PK, Ryle MJ, Monterosso GR, Liu J, Ballou DP, Hausinger RP. Steady-State and Transient Kinetic Analyses of Taurine/alpha-Ketoglutarate Dioxygenase: Effects of Oxygen

Concentration, Alternative Sulfonates, and Active-Site Variants on the FeIV-oxo Intermediate. Biochemistry. 2005; 44:3845–3855. [PubMed: 15751960]

47. Flagg SC, Giri N, Pektas S, Maroney MJ, Knapp MJ. Inverse Solvent Isotope Effects Demonstrate Slow Aquo Release from Hypoxia Inducible Factor-Prolyl Hydroxylase (PHD2). Biochemistry. 2012; 51:6654–6666. [PubMed: 22747465]
48. Neidig ML, Brown CD, Light KM, Fujimori DG, Nolan EM, Price JC, Barr EW, Bollinger JM, Krebs C, Walsh CT, Solomon EI. CD and MCD of CytC3 and taurine dioxygenase: role of the facial triad in alpha-KG-dependent oxygenases. J Amer Chem Soc. 2007; 129:14224–14231. [PubMed: 17967013]
49. Ryle MJ, Liu A, Muthukumaran RB, Ho RYN, Koehntop KD, McCracken J, Que L, Hausinger RP. O2- and alpha-Ketoglutarate-Dependent Tyrosyl Radical Formation in TauD, an alpha-Keto Acid-Dependent Non-Heme Iron Dioxygenase. Biochemistry. 2003; 42:1854–1862. [PubMed: 12590572]
50. Koehntop KD, Marimanikkuppam S, Ryle MJ, Hausinger RP. Self-hydroxylation of taurine/a-ketoglutarate dioxygenase: evidence for more than one oxygen activation mechanism. J Biol Inorg Chem. 2006:63–72. [PubMed: 16320009]
51. Tian GC. Effective Rate Constants and General Isotope Effect Equations for Steady-State Enzymatic-Reactions with Multiple Isotope-Sensitive Steps. Bioorg Chem. 1992; 20:95–106.

Appendix

As there are multiple isotope sensitive steps for the kinetic mechanism of FIH (Scheme 2), algebraic expressions for each kinetic parameter were derived using the net rate method of Tian.(51) The expression for $^{D2O}k_{cat}$ takes the form:

$$^{D2O}(k_{cat})=\frac{^{D2O}k_5+C_{Vf}+C_r\,^{D2O}K_5+^{D2O}k_{15}\left(\frac{k_5}{k_{15}}\right)}{1+C_{Vf}+C_r} \quad \text{(A1)}$$

$$C_{Vf}=k_5\left[\frac{k_8+k_9}{k_7k_9[O_2]}+\frac{1}{k_9}+\frac{1}{k_{11}}+\frac{1}{k_{15}}\right] \quad \text{(A2)}$$

$$C_r=k_6\left[\frac{1}{k_7[O_2]}+\frac{k_8}{k_7k_9[O_2]}\right] \quad \text{(A3)}$$

The parameters C_{Vf} and C_r are the forward and reverse commitments to catalysis. $^{D2O}k_5$ is the kinetic SIE for water release, $^{D2O}K_5$ is the equilibrium SIE on aquo release and $^{D2O}k_{15}$ the kinetic SIE on water re-binding. The equations derived for the SIEs for $k_{cat}/K_{M(CTAD)}$, $k_{cat}/K_{M(\alpha KG)High[CTAD]}$, $k_{cat}/K_{M(\alpha KG)Low[CTAD]}$ take similar form and are shown below.

$$^{D2O}\left(\frac{k_{cat}}{K_{M(\alpha KG)[HighCTAD]}}\right)=\frac{^{D2O}k_1\left(\frac{k_3[CTAD]}{k_2}\right)+^{D2O}K_1}{1+\frac{k_3[CTAD]}{k_2}} \quad \text{(A4)}$$

$$^{D2O}\left(\frac{k_{cat}}{K_{M(\alpha KG)[LowCTAD]}}\right)=\frac{^{D2O}k_1\left(\frac{k_3[CTAD]k_5}{k_2k_4}\right)+^{D2O}K_1\left(\frac{k_5}{k_4}\right)+^{D2O}k_5\,^{D2O}K_1+C_r\,^{D2O}K_1\,^{D2O}K_5}{1+C_f+C_r} \quad \text{(A5)}$$

$$C_f = k_5 \left(\frac{1}{k_4} + \frac{k_3}{k_2 k_4} \right) \quad \text{(A6)}$$

$$C_r = k_6 \left[\frac{1}{k_7[O_2]} + \frac{k_8}{k_7 k_9 [O_2]} \right] \quad \text{(A7)}$$

$$^{D2O}\left(\frac{k_{cat}}{K_{M(CTAD)}} \right) = \frac{^{D2O}k_5 + C_f + C_r{}^{D2O}K_5}{1 + C_f + C_r} \quad \text{(A8)}$$

$$C_f = \frac{k_5}{k_4} \quad \text{(A9)}$$

$$C_r = k_6 \left[\frac{1}{k_7[O_2]} + \frac{k_8}{k_7 k_9 [O_2]} \right] \quad \text{(A10)}$$

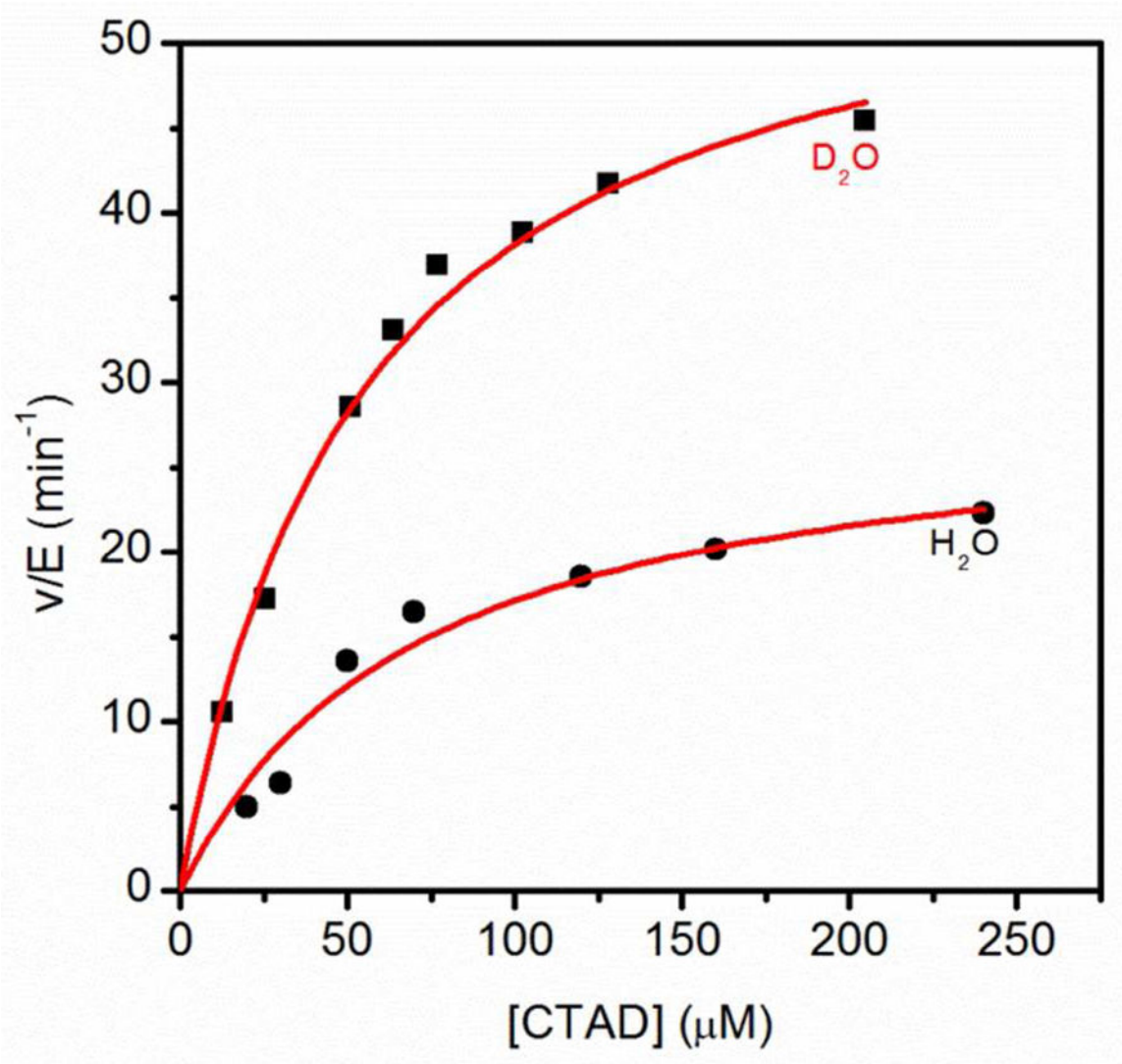

Fig. 1.

Steady-state kinetics of FIH in H_2O (●) and 97% D_2O (■) buffers. FIH (0.5 μM), ascorbate (2 mM), αKG (500 μM), $FeSO_4$ (50 μM) and CTAD (0–250 μM) were in 50mM HEPES pL 7.00.

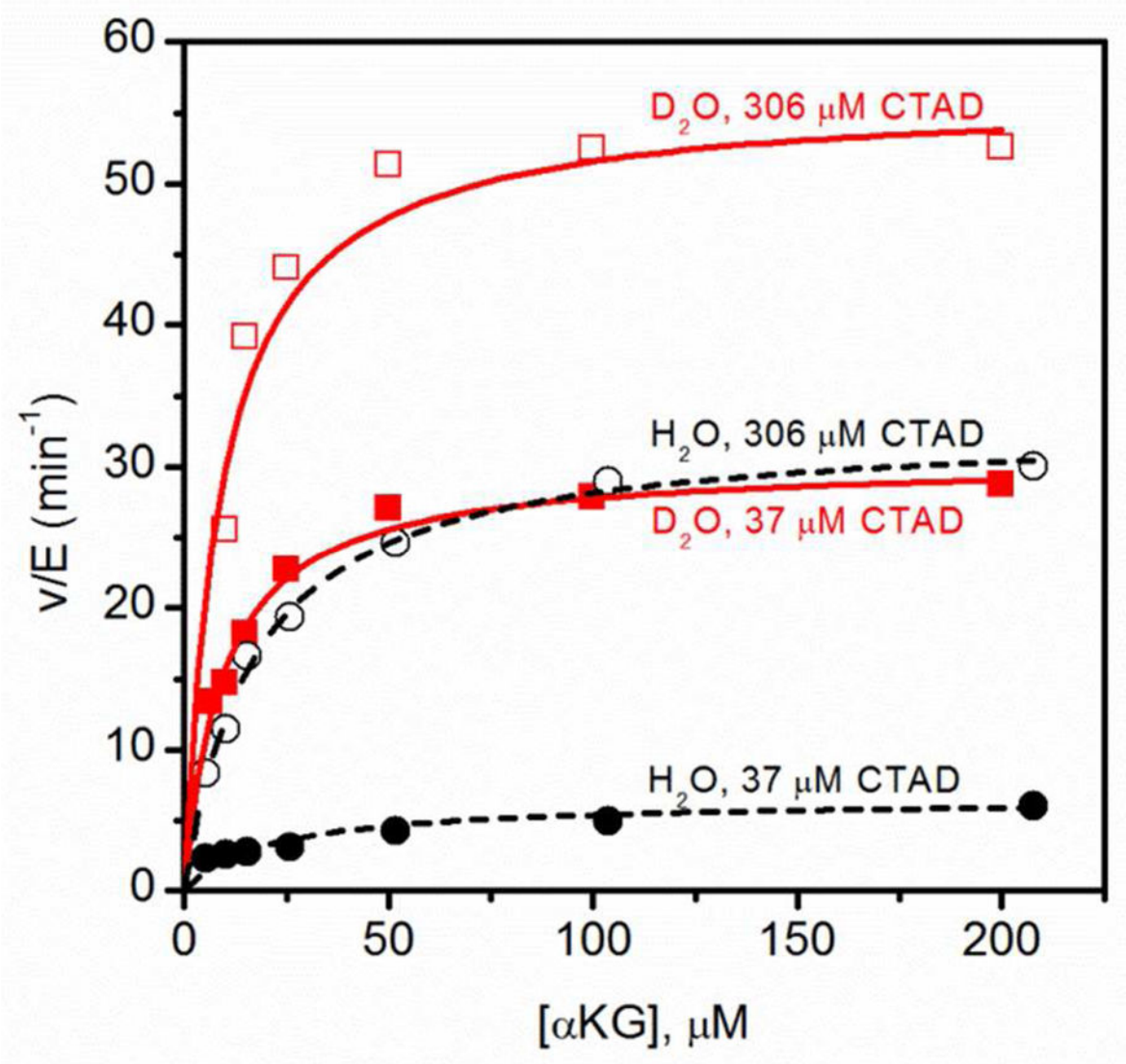

Fig. 2.

Steady-state kinetics of FIH for αKG at 37μM CTAD and 306μM CTAD, in H_2O (●,■) and D_2O(○,□)at 37.0°C. FIH (0.5μM), ascorbate (2 mM), αKG (0 – 210 μM), $FeSO_4$ (50 μM) and CTAD (37 μM and 306 μM) were in 50 mM HEPES pL 7.00.

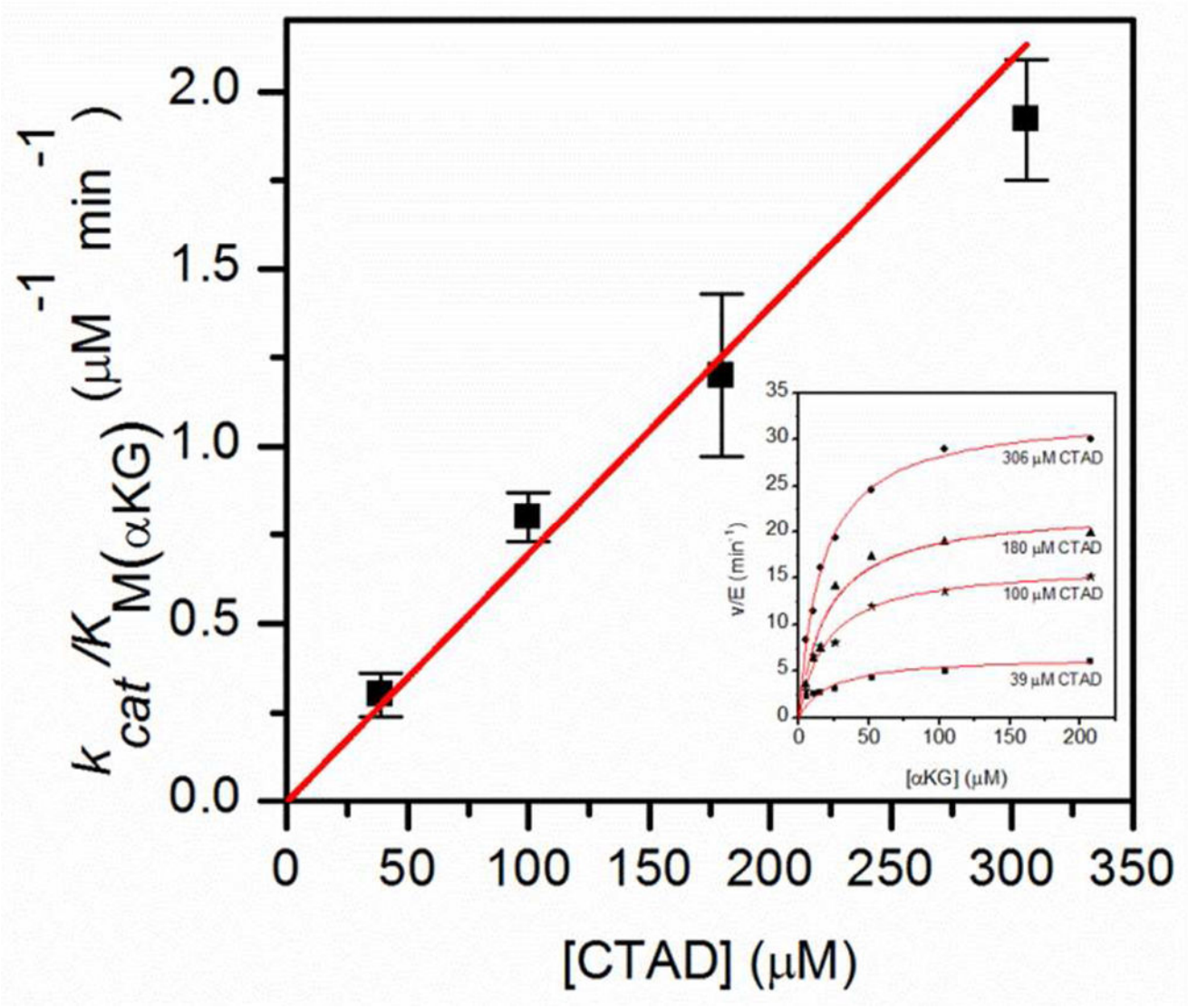

Fig. 3.

Regression plot showing $k_{cat}/K_{M(\alpha KG)}$ as a function of CTAD concentration. Inset: Steady-state kinetics of FIH with αKG as varied substrate, at different fixed CTAD concentrations at 37.0°C. FIH (0.5 μM), ascorbate (2 mM), αKG (0–210 μM), $FeSO_4$ (50 μM) and CTAD (39 – 306 μM) were in 50mM HEPES pH 7.00.

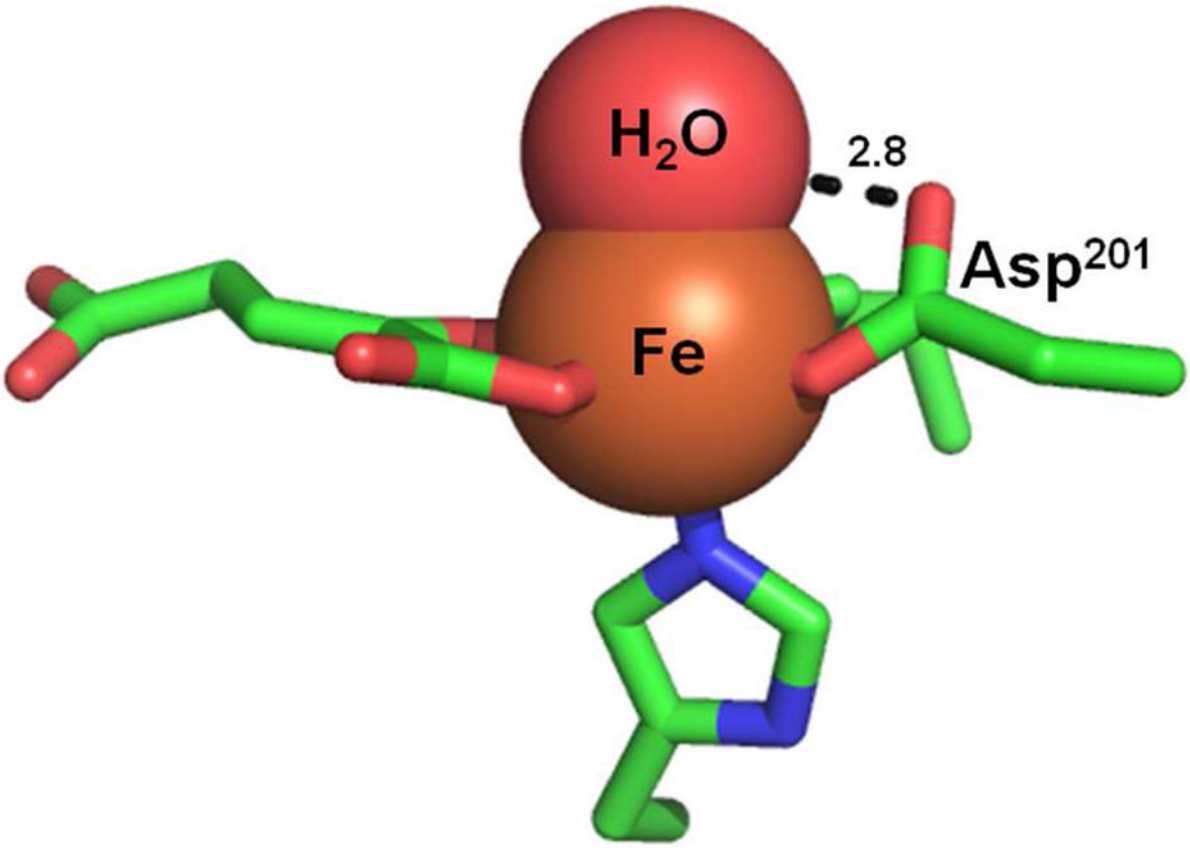

Fig. 4.
FIH active site with the 2.8 Å Asp^{201}-aquo hydrogen bond. (PDBID: 3P3P)

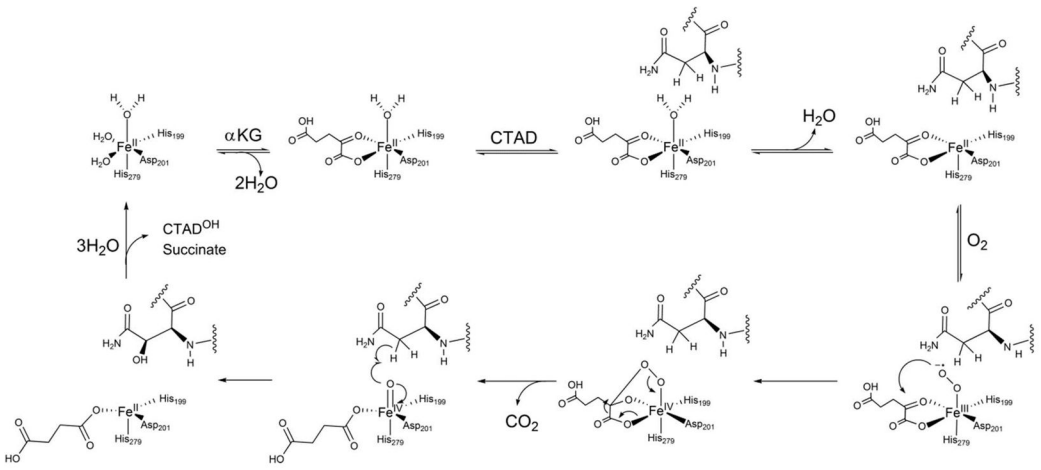

Scheme 1.

Consensus chemical mechanism for FIH.

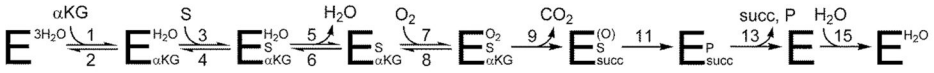

Scheme 2.

Proposed kinetic mechanism for FIH (*S* = CTAD).

Table 1

Solvent Isotope Effects for FIH. 50 mM HEPES pL 7.00, at 37.0°C.

	H_2O	D_2O	Experimental SIE	Theoretical SIE	# of Aquo Ligands
k_{cat} (min^{-1})[a]	30 ± 2.5	59 ± 2.0	0.51 ± 0.07	0.49	1
k_{cat}/K_{MCTAD} (μM^{-1} min^{-1})[a]	0.43 ± 0.10	1.09 ± 0.11	0.40 ± 0.07	0.49	1
$k_{cat}/K_{M\alpha KG(High[CTAD])}$ (μM^{-1} min^{-1})[b]	1.94 ± 0.13	6.05 ± 1.37	0.32 ± 0.08	0.24	2
$k_{cat}/K_{M\alpha KG(Low[CTAD])}$ (μM^{-1} min^{-1})[c]	0.29 ± 0.07	2.60 ± 0.34	0.11 ± 0.03	0.12	3

[a] CTAD as the varied substrate; FIH (0.5μM), ascorbate (2 mM), αKG (500 μM), $FeSO_4$ (50 μM), and CTAD (0 – 250 μM)

[b] αKG as the varied substrate; FIH (0.5μM), ascorbate (2 mM), αKG (5 – 200 μM), $FeSO_4$ (50 μM), and CTAD (306 μM)

[c] αKG as the varied substrate;FIH (0.5μM), ascorbate (2 mM), αKG (5 – 200 μM), $FeSO_4$ (50 μM), and CTAD (37 μM)

Table 2

Coupling of [Succinate] and [$CTAD^{OH}$] for FIH. 50 mM Tris pL 7.00, at 37.0°C.

	C^a
D_2O	1.1 ± 0.1[b]
H_2O	0.98 ± 0.03[c]

[a] $C = \frac{moles\ succinate}{moles\ CTAD^{OH}}$

[b] Reactions contained αKG (500 μM), $FeSO_4$ (50 μM), CTAD (200 μM) and FIH (5 μM) in 50 mM Tris pD 7.00

[c] Reference (14)